JOURNAL OF SPACECRAFT AND ROCKETS
Vol. 46, No. 4, July–August 2009

Preliminary Design of Vertical Takeoff Hopper Concept of Future Launchers Preparatory Program

G. Pezzella,* M. Marini,† and P. Roncioni‡
Italian Aerospace Research Centre—CIRA, 81043, Capua, Italy
J. Kauffmann§
ESA, 75015 Paris, France
and
C. Tomatis¶
Next Generation Launcher Prime, 10121 Torino, Italy

DOI: 10.2514/1.39193

This paper deals with the aerodynamic and aerothermodynamic preliminary design activities for the vertical takeoff hopper concept performed in the frame of the Future Launcher Preparatory Programme of the European Space Agency. The reentry scenario with the corresponding loading environment for the proposed vehicle concept is reported and analyzed. The hypersonic aerodynamic and aerothermodynamic characteristics of the vertical takeoff hopper are investigated by means of several engineering analyses and a limited number of computational fluid dynamics simulations in order to assess the accuracy of the simplified design estimations. The results show that the difference between Eulerian computational fluid dynamics and an engineering-based design is smaller than 10% for aerodynamic coefficients, whereas a margin of about 30% has to be taken into account for what concerns the aerothermodynamic results. The final results applicable for the prosecution of the launcher design activity are that, at the condition of peak heating, the vehicle features a nose stagnation point heat flux of about 500 kW/m² and an aerodynamic lift-to-drag ratio of about 1.2.

Nomenclature

B	=	wing span, m
C_D	=	drag coefficient
C_L	=	lift coefficient
C_m	=	pitching moment coefficient
c	=	distance along wing chord running from leading edge, m
D	=	aerodynamic drag, N
F	=	aerodynamic force, N
H	=	altitude, m
L	=	aerodynamic lift, N/fuselage length, m/chord length
M	=	Mach number/aerodynamic moment, Nm
Q	=	integrated heat load, MJ/m^2
$\dot{q}$	=	convective heat flux, kW/m^2
q	=	dynamic pressure, Pa
R	=	radius of curvature, m
Re	=	Reynolds number
Re/m	=	unit Reynolds number, 1/m
S	=	reference area, m^2
T	=	temperature, K
t	=	time, s
v	=	velocity, m/s
x	=	distance along vehicle forebody running from nose, m
α	=	angle of attack, deg
β	=	angle of side slip, deg
Λ	=	leading-edge sweep angle, deg
ρ	=	density, kg/m^3
ϕ	=	fuselage meridian angle, deg

Subscripts

eff	=	effective
N	=	nose
ref	=	reference
sp	=	stagnation point
WLE	=	wing leading edge
w	=	wall
Y	=	pitching moment
∞	=	freestream conditions

I. Introduction

IN THE frame of the Future Launchers Preparatory Program (FLPP), carried out by the European Space Agency (ESA), the vertical takeoff (VTO) hopper—reusable launch vehicle (RLV) concept is investigated [1]. The FLPP program is finalized to prepare Europe for the decision about the development of a next generation launcher (NGL) within the next decades [1,2]. The VTO hopper is a winged suborbital single stage rocket-powered vehicle booster designed for vertical takeoff [3]. Its mission goal is to carry an expendable upper stage (EUS), able to deliver a payload up to 8000 kg in geostationary transfer orbit (GTO), which is a mission design guideline for FLPP [1]. This reference mission is planned as a system requirement to meet the demand of the potential future market of commercial communication satellites with mass ranging from 4000 to 6000 kg in geostationary Earth orbit (GEO). In fact, the main objective of future European launchers is to satisfy the European institutional needs for low Earth orbit (LEO), mean Earth orbit (MEO), and GEO missions, corresponding to an equivalent performance of 8000 kg in GTO. Moreover, the capability of the launch system, corresponding to the institutional missions defined

Received 25 August 2008; revision received 7 May 2009; accepted for publication 15 May 2009.

*Ph.D. Research Engineer, Aerothermodynamics and Space Propulsion Lab, via Maiorise; g.pezzella@cira.it. Member AIAA.

†Ph.D. Research Engineer, Aerothermodynamics and Space Propulsion Lab, via Maiorise; m.marini@cira.it.

‡Ph.D. Research Engineer, Aerothermodynamics and Space Propulsion Lab, via Maiorise; p.roncioni@cira.it.

§Headquarters, FLPP Launch Systems Manager, ESA Launcher Directorate; jens.kauffmann@esa.int.

¶Launch Vehicle System Engineer; carlo.tomatis@nglauncher.net.

previously, to perform commercial missions is seen as an opportunity to support a cost efficient exploitation and is investigated as well [1]. The long-term scenario of the NGL foresees an initial operational capability of the FLPP vehicle not before 2020, assuming a development decision around 2013. Furthermore, it is presumed that a technology readiness level of 5–6 for the selected technologies will have to be reached at the time of the development decision. For the NGL an ambitious cost target has been defined with the requirement to reach a specific cost equal to one-third to one-half of Ariane 5 European Court of Auditors (ECA) specific cost in 2006 [1]. Within this framework, the paper goal is to show the current aerodynamic and aerothermodynamic analyses related to the VTO-hopper preliminary design activities. This effort was undertaken to assess the aerodynamic performance of the booster from reentry to landing, and to determine the aeroheating environment for the thermal protection system (TPS) design, because several vehicle concepts are under investigation in the frame of FLPP concepts competition [2]. To this scope the nominal reentry scenario with the corresponding loading environment for the proposed vehicle concept is reported and analyzed. Different design and analysis approaches have been addressed. In fact, concept aerodynamics and aerothermodynamics have been assessed both by means of several engineering-based methods and more reliable computational fluid dynamics (CFD) analyses. Indeed, design activities have been performed starting from engineering-based methods, in order to rapidly accomplish the launcher aerodynamics and aerothermodynamics, thus generating a number of possible reentry trajectories able to fulfill the program requirements. In fact, in the early design stages, which require very rapid turnaround of environments for trade studies, it is most cost effective to supplement accurate design analyses with simplified methodologies.

Within engineering-based aerodynamic and aerothermodynamic analyses, a widely employed design tool is a 3-D panel method code developed by Centro Italiano Ricerche Aerospaziali (CIRA). This code performs aerodynamic analyses by means of local inclination methods, typical of hypersonics, whereas the heat flux distributions on the vehicle configuration have been evaluated by means of improved boundary-layer methods. Then, increasing the order of complexity, a number of detailed 3-D Euler and Navier–Stokes CFD analyses have been performed for different flight conditions along the descent trajectory. CFD computations are needed to anchor engineering estimations and to properly model the vehicle's environment, when predicting surface properties in localized surface areas of topological complexity or areas affected by shock interaction (i.e., wing and tail leading edges). The results show that the booster aerodynamics and aerothermodynamics, derived from the engineering design approach, are sufficiently accurate for preliminary analysis purposes. Finally, the results applicable for the prosecution of the FLPP design activity, carried out by ESA, are summarized.

II. VTO-Hopper Vehicle Concept and Mission

The VTO-hopper vehicle architecture in clean aerodynamic configuration (i.e., controls in neutral position) is shown in Fig. 1, both for the ascent (on the left) and the descent phase (right side), respectively.

It is a two-stage-to-orbit space transportation system made up of an EUS and a fully reusable first stage (namely, booster), which is under investigation in this paper. The booster shape features a rather conventional slender missilelike configuration layout, a circular cross-section fuselage with a loft fillet on the belly side to accommodate the wing, delta planform wings in the rear position (45.17 deg leading-edge sweep), and a central vertical stabilizer. The circular cross section is constant up to the fuselage-wing interface, where the wing is blended into the fuselage to minimize wing-body interference heating, and is adapted in order to introduce the body flap. Some details of the vehicle concept are given in Table 1.

Table 1 VTO hopper configuration details

Airfoil data	
Relative thickness	7.5%
Relative leading-edge radius	4.5%
Relative camber	0% (no camber)
Wing geometry data	
Root/tip chord, m	17.70/7.53
Half span $B/2$, m	15.9
Wing leading-/trailing-edge angle, deg	45.17/13.7
Angle of incidence of the wing, deg	3
Dihedral, deg	3

The booster forebody is characterized by a simple cone–sphere configuration, with smooth streamlined surfaces in the upper and lower sides of the fuselage to prevent local dangerous overheating, and with a fuselage nose radius (R_N) equal to 1 m. The aerodynamic control surfaces comprise rudders on the vertical tail, elevons and ailerons on the wings, and a body flap underneath the main engines to provide maneuverability and longitudinal stability during the atmospheric descent [i.e., an aerodynamic surface behind the vehicle center of gravity (CoG) balances the nose up pitching moment, typical of such kind of vehicle configuration at hypersonic speeds].

The VTO-hopper mission starts from the Guyana Space Centre, where the vehicle lifts off vertically with all five engines running and performs a parabolic suborbital trajectory. After main engine cutoff: $H > 90$ km, $v > 5$ km/s), the upper stage separates from the reusable booster, ignites and transports the payload into the final target GTO orbit. The reference mission for FLPP consists of the injection of a 8000 kg payload into GTO.

After the staging, the reusable booster will perform a ballistic arc trajectory, followed by a gliding downrange reentry flight to a landing site 4500 km far from the launch site, and land horizontally.

The reentry phase is guided by a drag-velocity profile and is controlled by modulating the angle of attack (AoA) and the bank angle throughout the descent flight. When entering the more dense layers of the atmosphere the aerodynamic forces rapidly increase, finally stabilizing the VTO attitude. Hence, a number of trajectory constraints have been considered, thus defining the admissible reentry corridor of the booster. For instance, the dynamic pressure stays below 45 kPa, the heat flux at stagnation point does not exceed 500 kW/m^2, the total load factor is smaller than 4.5, and the equilibrium glide boundary margin is 30 deg.

Once the reentry corridor is defined, the simulation of the return of the VTO is performed under a closed control loop with parametrical variation of the initial banking maneuver. The banking is automatically controlled to a flight direction with minimum distance to the launch site. The reentry mission analyses are performed using the

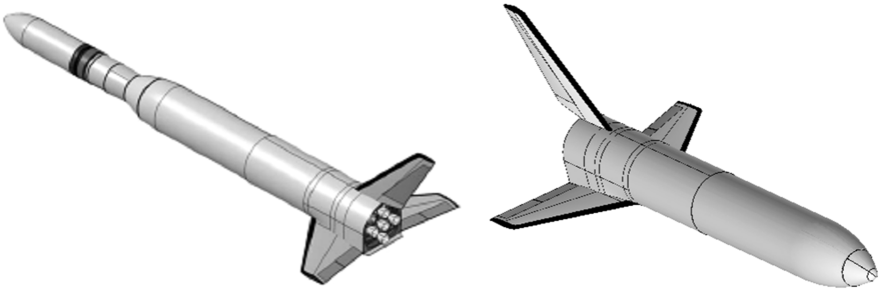

Fig. 1 The VTO hopper configuration; left: complete vehicle; right: reusable booster stage.

point-mass scheme, with 3 translational degrees of freedom, and the system equations of motion are derived from the classic two-body dynamics approach.

Flight mechanic analyses resulted in the reentry scenario for the VTO-hopper booster, illustrated in Figs. 2 and 3 [4]. This represents the VTO nominal reentry scenario investigated to build up both the aerodynamic database (AEDB) and the aerothermodynamic database (ATDB) of the FLPP booster concept.

The initial conditions of the descent flight are summarized in Table 2.

Note that the initial conditions of reentry are most important because the maximum loads experienced during descent show a high sensitivity according to a change in separation conditions (e.g., flight path angle and velocity at entry interface are of strongest influence) [4].

Figure 2 shows the altitude versus reentry time from the entry interface (e.g., 120 km) to terminal area energy management, fixed at 20 km altitude.The Mach and AoA time histories are also reported. Figure 3 displays the flight profile in terms of an altitude-velocity map. The constant Mach and Reynolds numbers lines are included in the figure to properly characterize the aerodynamic flight scenario of the booster.

Several Mach numbers ranging from 2 to 20 and five Reynolds numbers (i.e., $[1, 3, 8, 20, 70] \times 10^6$) with respect to the vehicle's L_{ref} have been considered for the simulations, as displayed in Fig. 3. It must be noted that the ranges of Mach and Reynolds numbers have been selected to cover a wide part of the reentry flight, especially the most critical one from the aeroheating point of view (i.e., $M_\infty = 13.4$).

Table 2 Initial conditions of reentry flight [4]

Altitude, m	120×10^3
Latitude, °	1.666
Longitude, °	−38.25
Velocity, m/s	4969
Flight path angle, deg	−6.604
Vehicle mass, kg	94×10^3

III. Description of Design Approach and Numerical Tools

The VTO-hopper design analyses, summarized in this paper, are aimed to carry out a preliminary AEDB for the flight mechanics analysis, and ATDB for the TPS sizing activities, in compliance with the phase-0 design level. The aerodynamic coefficients are provided as a function of Mach number and AoA (zero sideslip angle and no active control surface deflections) according to the "space-based" design approach [5,6].

On the other hand, the heat fluxes have been computed for a number of selected points along the vehicle reentry trajectory, as

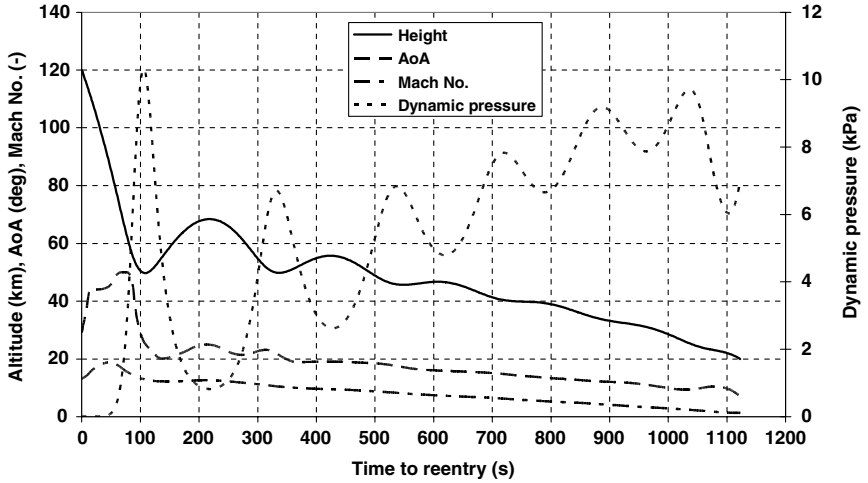

Fig. 2 The VTO hopper reentry scenario: altitude, Mach, dynamic pressure, and AoA time histories.

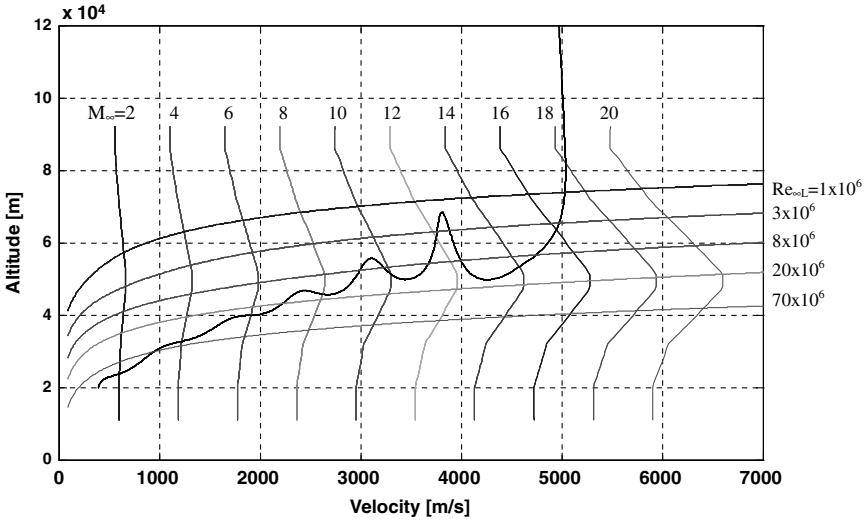

Fig. 3 The VTO hopper reentry trajectory. Altitude-velocity map.

prescribed by the "trajectory-based" design approach [5,6]. The first one (AEDB) foresees the generation of a complete data set as function of a number of independent parameters (i.e., M_∞, Re_∞, α, and β); the second one (ATDB) consists of performing the aerothermal computations at a finite number of "critical" points on a given nominal design trajectory. Note that, being at an early stage of vehicle design, the flow computations and TPS thermal response evaluations are performed in an uncoupled manner. Indeed, aerothermal analyses are performed at several time points on the reentry trajectory, assuming a nonconducting thermal protection material (TPM).

In both cases (i.e., aerodynamics and aerothermodynamics), the advantage of using an engineering-based design approach is that one can rapidly develop both AEDB and ATDB databases as a function of the freestream conditions in a matter of hours, as vehicle configuration and mission requirements evolve. In fact, even if it is very tempting to select a large number of points to perform calculations, a large number of CFD simulations will prove neither cost effective nor timely in the preliminary design stage in which quick turnaround estimates are a must.

In the present analysis only the continuum regime (at supersonic and hypersonic speed ranges) with the air modeled both as perfect and as equilibrium gas has been studied. Moreover, considering that important issues affecting the vehicle convective heating are transition and turbulence, aeroheating analyses at the launcher wall are provided both for laminar and turbulent flows. Neither rarefaction nor real gas effects were accounted for.

It is worth nothing, however, that at high altitudes the rarefaction and real gas effects should be taken into account when the vehicle is flying at high Mach number, being the AEDB and ATDB are strongly affected. Therefore, these aspects would have to be considered for the next phases of vehicle design.

In the following paragraphs the tools used for the design analyses are described.

The VTO hopper shows a number of severe flight conditions for which analyses are required. It must return from 120 km, fly trimmed throughout hypersonic and supersonic regimes until landing, and withstand severe aeroheating. An accurate aerodynamic and aerothermodynamic analysis of all these flight conditions is very complex and time consuming, and not compatible with a phase-0 design study, for which fast predicting methods are requested. Therefore, the evaluations of the vehicle AEDB and of its reentry aerothermal environment have been mainly performed by means of engineering tools, while a limited number of accurate CFD computations have been carried out to verify the attained accuracy, and to focus on some critical design aspects not predictable with simplified tools.

Engineering-based aerodynamic and aerothermodynamic analyses have been extensively performed by using a 3-D panel method code developed by CIRA (SIM, surface impact method) in the frame of its research activities on preliminary design of reentry vehicles [7,8]. This tool, at high supersonic and hypersonic speeds, is able to assess the AEDB and ATDB of a complex reentry vehicle configuration by using simplified approaches as local surface inclination methods and approximate boundary-layer methods, respectively. Surface impact methods, typical of hypersonics, are based on Newtonian, modified Newtonian, tangent cone, and tangent wedge theories. The heat flux calculations have been performed using also simplified engineering formulas such as Detra, Kemp, and Riddell (DKR) and Gomg relationships, to confirm and integrate the tool results (heat loads) at the most critical parts of the vehicle (e.g., vehicle nose and wing leading edges) [6,9,10].

The engineering codes perform the aerothermal analysis of the vehicle configurations based on the surface streamlines. The streamlines are generated starting from the inviscid surface velocities generated in the aerodynamic analysis phase. Once the streamlines are provided, the aeroheating analysis is performed along each streamline by using a simple one-dimensional boundary-layer method (1-D BLM).

When a perfect gas model is chosen, the thermodynamic and transport properties are calculated with ideal gas equations. The gas is assumed to be thermally and calorically perfect, and Sutherland viscosity is used with a constant Prandtl number. To compute heat fluxes in equilibrium gas conditions, the thermodynamic and transport properties of air are evaluated by means of Tannehill's curve fits [11]. The generic vehicle component may be modeled as either a flat plate or a leading edge by selecting the appropriate boundary-layer model. The most commonly used flat-plate methods for both laminar and turbulent flow are Eckert's reference enthalpy and, in addition, the method of Spalding and Chi is used for turbulent flow [12].

In Fig. 4 a typical mesh surface of the VTO used for the engineering evaluations is shown. The surface grids are created by using ICEM-CFD©.

On the other hand, the numerical code used to carry out the CFD analyses of the VTO vehicle is the CIRA code H3NS that computes inviscid and viscous solutions for perfect gas and reacting gas flows in either an equilibrium or a nonequilibrium state, with a finite volume approach. Tannehill's curve fits are used for the thermodynamic and transport properties of equilibrium air [11].

A flux difference splitting upwind scheme is used for the convective terms, with a second-order essentially non-oscillatory-like reconstruction of cell interface values [8]. The viscous fluxes are calculated by central differencing, i.e., computing the gradients of flow variables at cell interfaces by means of Gauss theorem. Time integration is performed by employing an Euler forward scheme coupled with a point implicit treatment of the species and vibration energies source terms. Both sequential and parallel versions of the code are currently available.

Several boundary conditions can be applied for the viscous computations, including different catalycity models and the possibility to assign at the wall a fixed temperature or a radiative equilibrium condition.

CFD computations have been carried out on a multiblock structured grid (shown in Fig. 5) generated by means of the commercial ICEM-CFD tool. The grid used for CFD calculations consisted of 62 blocks for an overall number of about 2×10^6 cells (half-body). Each computational grid has been tailored for the freestream conditions of the trajectory control points, reported in Sec. VI. A great deal of care was taken in multiblock grid development. In fact, the distribution of surface grid points has been dictated by the level of resolution desired in various areas of a vehicle such as stagnation region and base fillet, according to the computational scopes. A close-up view of 3-D mesh on the vehicle surface can be seen on the right side of Fig. 5.

To obtain a good quality Navier–Stokes solution, the mesh has been built clustering the points as close as possible to the vehicle's surface. Moreover, attention has been paid to grid density, grid distribution (stretching), and cell Reynolds number at the wall, because heat flux prediction is very sensitive to those mesh features. Grid refinement in strong gradient regions of the flowfield has been made through a solution adaptive approach and multigrid techniques are used to accelerate convergence.

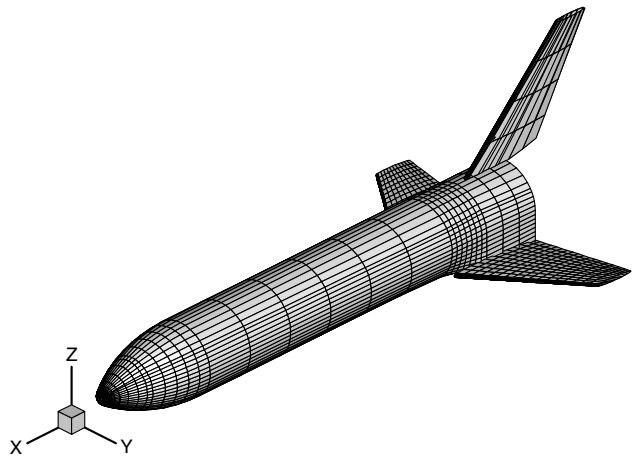

Fig. 4 The booster's surface mesh used for engineering analyses.

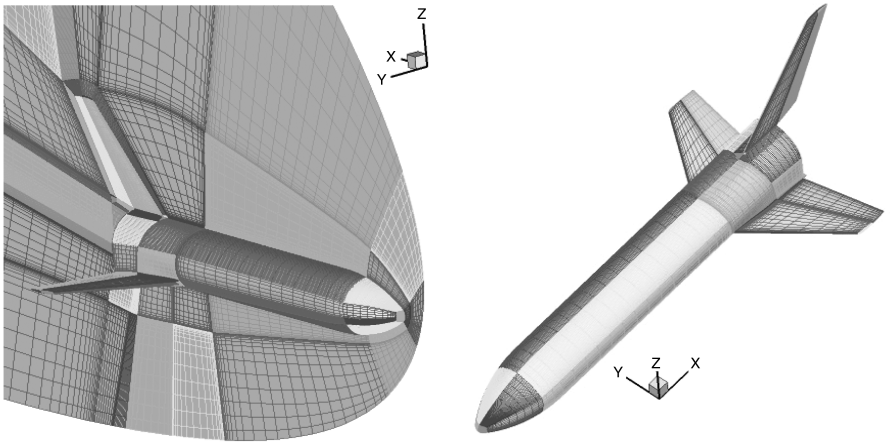

Fig. 5 The multiblock CFD domain. Mesh on symmetry plane and on vehicle surface.

IV. VTO Hopper Aerodynamic Analysis

The aerodynamic analysis is shown in terms of lift C_L, drag C_D, and pitching moment C_m coefficients which are calculated according to Eqs. (1) and (2), respectively,

$$C_i = \frac{F_i}{(1/2)\rho_\infty v_\infty^2 S_{\text{ref}}} \qquad i = L, D \tag{1}$$

$$C_m = \frac{M_y}{(1/2)\rho_\infty v_\infty^2 L_{\text{ref}} S_{\text{ref}}} \tag{2}$$

The reference parameters selected to make aerodynamic forces and moments nondimensional coefficients are as follows:

1) $L_{\text{ref}} = 58.8$ (m) (longitudinal reference length);
2) $S_{\text{ref}} = 193.23$ (m^2) (planform area of wetted wing).

The point for aerodynamic moment calculation is fixed at the vehicle nose.

Based on the reentry flight scenario summarized in Fig. 3, the aerodynamic data set has been generated for the following ranges:

1) $2 < M < 20$ [2, 3, 5, 7, 10, 15, 20];
2) 0 deg $< \alpha <$ 50 deg [0, 5, 10, 15, 20, 25, 30, 35, 40, 45, 50];
3) $10^6 < Re < 70 \times 10^6$ $[1, 3, 8, 20, 70] \times 10^6$;
4) $\beta = 0$ deg.

These ranges are compliant to a space-based design approach in the sense that the vehicle aerodynamic performances are evaluated at a number of flight conditions large enough to accommodate or enclose all possible vehicle reentry trajectories (i.e., trajectory dispersion envelope). Neither lateral directional analysis nor wing and body flap effects have been taken into account in these analyses. Note that for the aerodynamic coefficients the usual flight mechanics convention is adopted.

For each Mach number, aerodynamic data are provided to flight mechanics both in tabular and diagram form. All data refer to viscous analyses. As an example of the engineering aerodynamic database of the VTO hopper concept in clean configuration, results for $M_\infty = 7$ are summarized in Fig. 6, where the pressure coefficient distribution over the wetted vehicle surface for two AoAs (i.e., 10 and 30 deg) is reported.

Ranging AoA from 10 to 30 deg, as highlighted by pressure coefficient contours, the hopper configuration exhibits an enhanced aerodynamic performance, because both lift and drag coefficients increase about 5 times, respectively.

In particular, Fig. 7 shows that starting from AoA = 0 deg the VTO hopper aerodynamic efficiency straightly increases reaching a peak of about 1.6 at AoA = 17 deg, and then it decreases to about 0.9 at AoA = 40 deg. These results include viscous effects and have been evaluated for a dynamic pressure equal to about 5.2 kPa.

The pitching moment coefficient refers to the vehicle CoG located at 69.4% of the VTO fuselage length (e.g., $x_{\text{CoG}} = 40.82$ m from the nose). As shown, the vehicle is statically stable (e.g., $C_{m\alpha} = \partial C_m/\partial\alpha < 0$) for AoA higher than 25 deg; anyway, to trim the booster, the aerodynamic control surfaces have to balance a pitching moment coefficient lower than about 0.05, depending on the AoA.

A similar behavior (due to the effects of AoA) can be expected for the heat flux distribution within the aerothermodynamic analysis and will be shown hereafter.

V. VTO Hopper Aerothermodynamic Analysis

Once the reentry scenario is provided, it follows the aeroheating environment that the VTO hopper has to withstand along its lifting reentry flight. By flying, in fact, the work done by aerodynamic drag in braking the vehicle heats the surface with a severity that depends on the reentry vehicle configuration. Therefore, stagnation points on the vehicle fuselage, and on three different wing sections have been monitored as reference control points (see Fig. 11), to characterize the VTO hopper aerothermal environment. Note that the aeroheating environment at these key points, known also as body points, is integrated as constraint into the reentry trajectory calculation because no violations of TPS temperature limits are allowable.

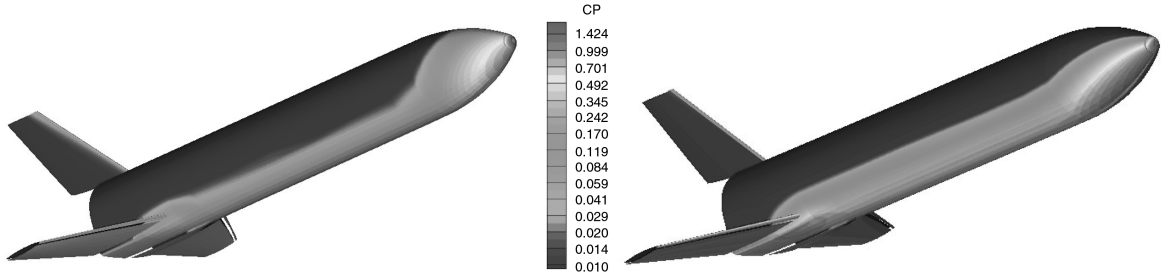

AoA= 10 deg **AoA= 30 deg**

Fig. 6 Pressure coefficient contours on the vehicle surface at $M_\infty = 7$.

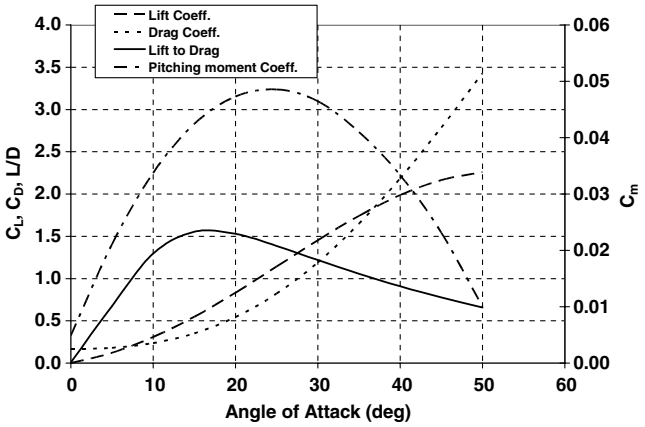

Fig. 7 Aerodynamic characteristics and pitching moment coefficient at $M_\infty = 7$.

As done in the aerodynamic analysis, only engineering methods have been used to assess the preliminary ATDB of the booster concept. To build the heat transfer profile for the fuselage stagnation point the DKR formula has been employed [6]:

$$\dot{q} = \frac{1830}{\sqrt{R_N}} \rho_\infty^{0.5} \left(\frac{v_\infty}{10^4}\right)^{3.05} \tag{3}$$

while the Gomg's relationship is applied for the wing leading edge (WLE) [10]:

$$\dot{q}_{\text{WLE}} = \frac{1}{\sqrt{2}} \frac{1}{\sqrt{R_{\text{WLE}}}} \dot{q}_{R_N=1} \cos^{1.2} \Lambda_{\text{eff}} \tag{4}$$

where Λ_{eff} is the effective sweep angle:

$$\sin \Lambda_{\text{eff}} = \sin \Lambda \cos \alpha \tag{5}$$

$$\cos \Lambda_{\text{eff}} = \sqrt{1 - \sin^2 \Lambda_{\text{eff}}} \tag{6}$$

It is worth mentioning that this analysis is reasonable and applicable in the continuum flow regime only.

In Fig. 8 the time histories of the aerothermal environment at the booster's nose and at the stagnation point of each wing control section are shown. As one can see the reentry trajectory results in a peak heating at the fuselage nose of about 500 kW/m^2, reached when the VTO launcher is flying at $M_\infty = 13.4$, and the AoA is nearly equal to 30 deg, at an altitude of 50.8 km (e.g., $q_\infty \cong 10$ kPa).

On the other hand, looking at what happens to the wings, Fig. 8 highlights the fact that the spanwise distribution of heat flux at WLE is expected to increase ranging from wing root to tip due to the smaller WLE radius (relative leading-edge radius of 4.5%), and that the wing shape (e.g., wing sweep angle and wing leading-edge radius profile in spanwise) is characterized by an aeroheating at leading edge that reaches values close to that of the fuselage nose.

The heating profiles, reported previously, lead to an integrated heat load Q that is expressed by

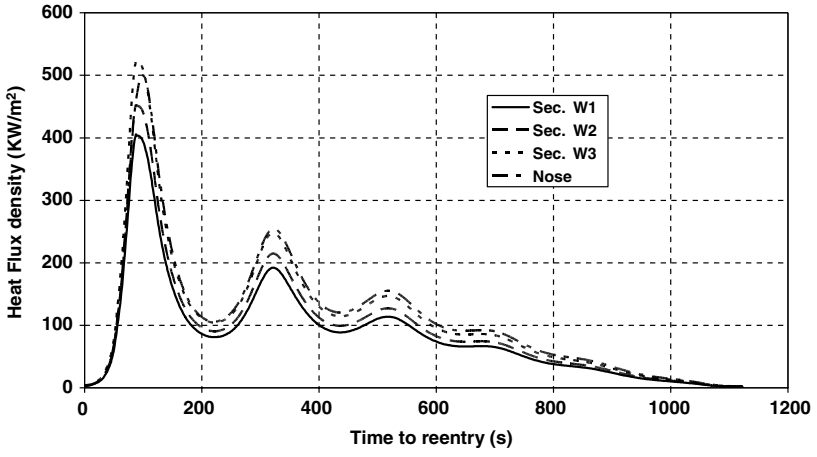

Fig. 8 The aeroheating environment vs entry interface time at nose and WLE of Secs. W1, W2, and W3.

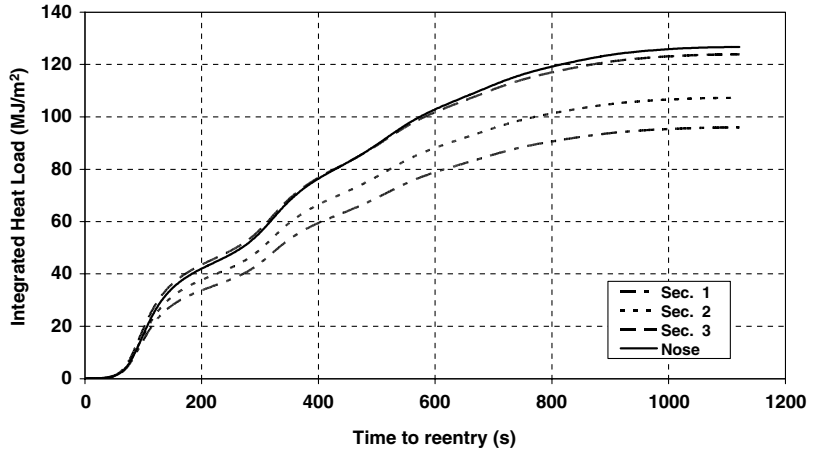

Fig. 9 VTO hopper heat load profiles for nose and for wing sections.

Table 3 Control point freestream conditions

Control points	H, m	M, −	AoA, deg	q_∞, kPa	Re/m, 1/m
1	81,100	18.0	47.7	0.2	5962.9
Peak heating 2	50,800	13.4	29.7	9.7	241,204.6
3	68,300	12.6	24.8	0.8	27,215.2
4	50,000	10.6	22.3	6.7	210,306.4
5	46,500	8.5	18.0	6.6	264,465.9

$$Q_{\mathrm{sp}}(t) = \int_{t_E}^{t} \dot{q}_{\mathrm{sp}}(\tau)\mathrm{d}\tau \tag{7}$$

where t_E is the time instant corresponding to the entry point, when the vehicle begins the reentry. The time histories of the heat load per unit area (MJ/m^2) for nose and wing sections, according to Eq. (7), are reported in Fig. 9.

Note that both heat flux and integrated heat load are fundamental for the TPS design analyses. The heat flux distribution on the aeroshape dictates both the selection of TPM, able to withstand the heat rate, and the TPS configuration; the integrated heat load suggests the thermal shield thickness.

As far as the heat flux distribution over the vehicle surface (only fuselage and wing) is concerned, a number of trajectory flight conditions (trajectory control points) have been considered, in the framework of a trajectory-based design approach [5,6]. Figure 10 gives an overview of the trajectory zone where control points (CP) have been established, while their freestream conditions are reported in Table 3. The design points are selected on the trajectory in such a way to duplicate the area under the peak heating. In addition to heat pulse (CP 2), the other points selected included the maximum AoA (CP 1) and a point at which the Mach is relatively high and the AoA is low (CP 5). This last point could be critical from the point of view of shock–shock interaction (SSI) at the vertical stabilizer leading edge.

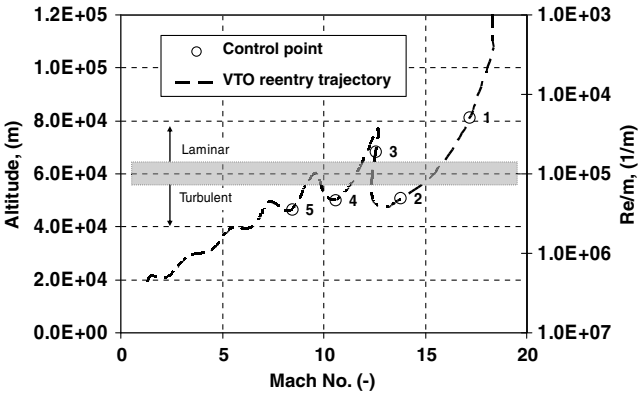

Fig. 10 Heat flux control points in the H-M_∞-Re/m space.

The engineering aerothermodynamic database of the VTO hopper concept in clean configuration provides vehicle thermal loading by means of heat flux profiles over vehicle surface, at each design point summarized in Table 3.

To facilitate the comparison among the results and the application for TPS sizing, the heat fluxes have been provided along selected section lines of fuselage and wing. As shown in Fig. 11, five slices have been selected on the fuselage whereas three slices have been selected on the wing surface.

Finally, numerical computations herein reported refer to air in chemical equilibrium with vehicle cold wall ($T_w = 300$ K) boundary conditions, as a conservative estimation. Indeed, the equilibrium flow solution represents a good approximation to a nonequilibrium one with a fully catalytic wall boundary condition, and a difference from the latter can be easily evaluated at the engineering level. We regard the equilibrium condition as resulting in the maximum heat flux, confirming that it is largely used as the reference condition for TPS design [13].

Moreover, considering that the laminar-turbulent transition strongly affects the heat fluxes, for what concerns the state of the boundary layer to be used in aeroheating calculations, Fig. 10 highlights that, during descent, VTO is going to experience strong effects of Reynolds and Mach numbers. The shaded region in Fig. 10 refers to unit Reynolds equal to 10^5 1/m, above which the flow is assumed fully turbulent. Thus, a selected CP lying above this boundary requires a turbulent flow computation in addition to a laminar one.

The following plots show the results obtained at trajectory CPs 2, 4, and 5, compared on the fuselage centerline (Secs. B1 and B5 of Fig. 11), and on wing section W1, to characterize the fuselage and wing thermal loading.

Figures 12 and 13 show the heat flux along the fuselage centerline as evaluated at CPs 2 and 5 (see Table 3 for CP's freestream conditions).

When comparing the results obtained at different AoA, it results that at AoA = 18 deg the vehicle leeside reaches a rather large heat flux, while at AoA = 30 deg, as expected, the windside is the most

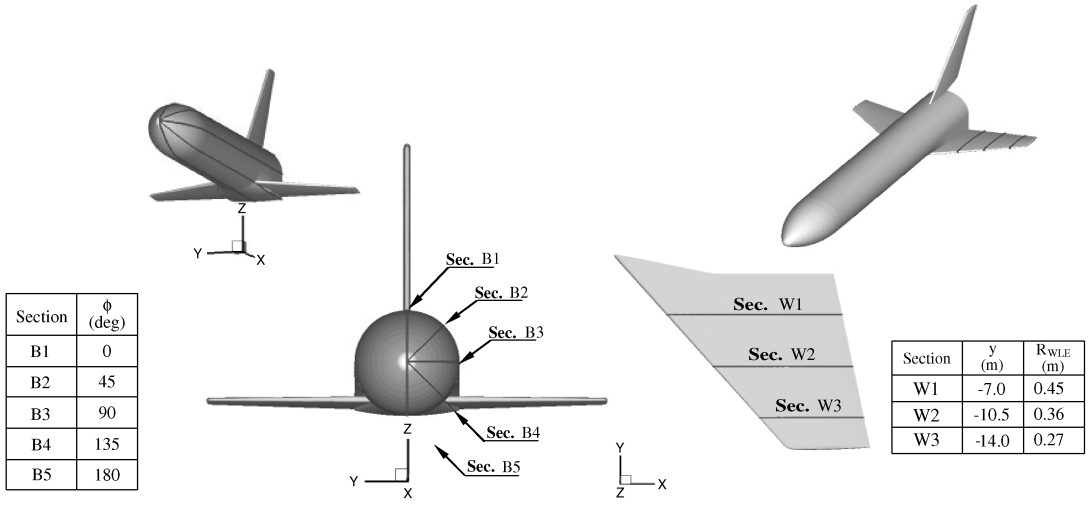

Section	ϕ (deg)
B1	0
B2	45
B3	90
B4	135
B5	180

Section	y (m)	R_{WLE} (m)
W1	-7.0	0.45
W2	-10.5	0.36
W3	-14.0	0.27

Fig. 11 VTO hopper fuselage and wing sections where heat fluxes are provided.

solicited vehicle part. Note, in particular, that because the bow shock is very close to the fuselage stagnation region (as will be shown in Sec. VI), here the flow is expected to be frozen so that no chemistry effects apply. Moreover, the flow near the stagnation point is expected to be laminar because of the low Reynolds number and the favorable pressure gradient [14].

As far as aeroheating on the wing leading edge is concerned, Figs. 14 and 15 show the heat flux along Sec. W1 as evaluated at CPs 2 and 4 (see Table 3), thus showing a large effect of turbulence (up to 5 times the laminar heating on the airfoil windside).

In conclusion, Figs. 12–15 show mainly two areas of high heating: the forebody stagnation point and the wing leading edge. For both, on the windward surface the equilibrium flow model produces generally higher thermal loads in the case of turbulent boundary layer. Roughly, a ratio of 3–4 is estimated between turbulent and laminar flow assumption, both at vehicle windside and leeside. It must be stressed, however, that these aeroheating results have not been obtained by means of accurate and more reliable CFD computations. Therefore, a proper margin should be adopted in recognizing vehicle aerothermodynamic data. This is especially true when considering aeroheating estimates on wing, as will be clarified hereafter, because the effect of the interaction between bow and wing shocks (e.g., SSI) is not taken into account. As is well known, SSI determines an intense

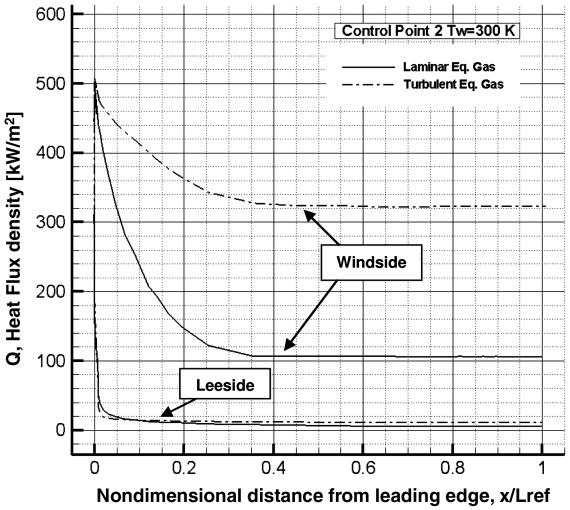

Fig. 12 Centerline heat flux (Secs. B1, B5) at CP 2, for laminar and turbulent equilibrium flow.

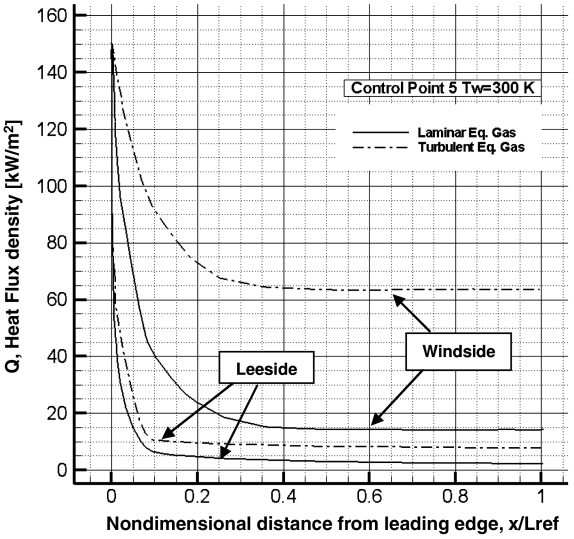

Fig. 13 Centerline heat flux (Secs. B1, B5) at CP 5, for laminar and turbulent equilibrium flow.

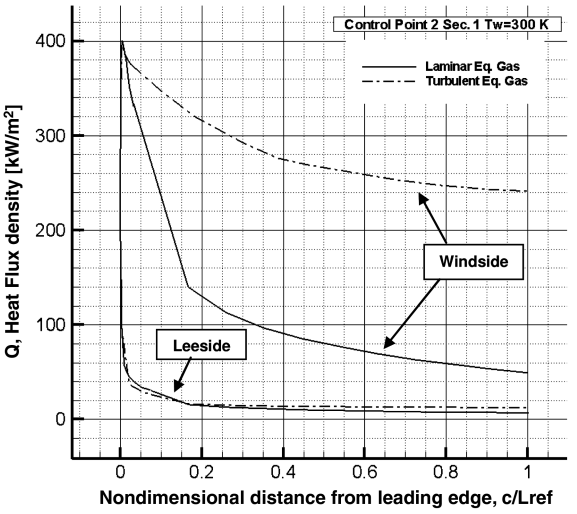

Fig. 14 Airfoil heat flux at Sec. W1 at CP 2, for laminar and turbulent equilibrium flow.

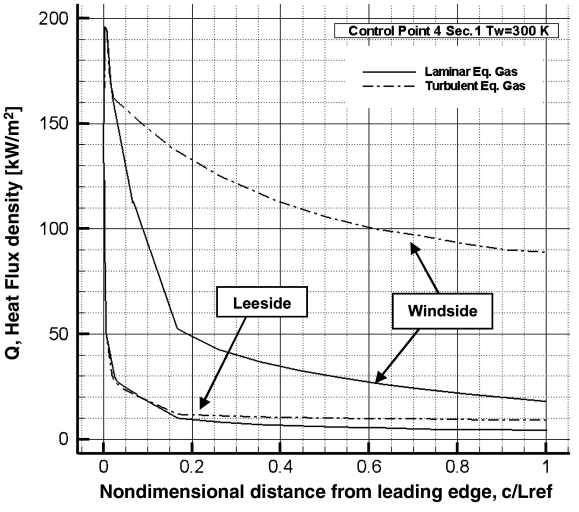

Fig. 15 Airfoil heat flux at Sec. W1 at CP 4, for laminar and turbulent equilibrium flow.

local overheating that must be accurately predicted for a reliable wing TPS design. The location of this overheating depends on several factors as freestream conditions (i.e., M_∞, AoA) and flow conditions. In fact, different modeling of real gas effects produces different shock topologies, which yield different spatial distributions of heating along the wing leading edge.

Anyway, by analyzing these figures, very interesting features can be taken into account for a reliable TPS design for the VTO hopper concept. For example, due to the steep reentry, the booster experiences a short heat pulse on its windward side, which drives maximum heat flux and surface temperature to levels comparable to RLVs reentering from LEO; the short heat pulse on the windward side is manageable with ceramic hardcover TPS, but restricts the application of specifically lighter metallic TPS, a dramatic effect of turbulence on vehicle windside aeroheating.

VI. Reliability of Design Activities

To assess the error margins of engineering-based design analyses, several comparisons are provided between engineering results, summarized previously, and data provided by more reliable CFD computations.

To this scope a number of flight conditions have been selected to carry out CFD Euler and Navier–Stokes computations. Those numerical computations allow anchoring the engineering analyses

and focusing on some critical design aspects not predictable by means of engineering tools. The selected control points are reported in Fig. 16.

Each CP lies within the flight scenario foreseen for a typical mission profile of the booster (according to the space-based design approach).

CFD numerical computations confirm that the flowfield is dominated by the gas chemistry conditions. For example, Fig. 17 shows the Mach number contours in a booster cross plane for the perfect gas (on the left) and equilibrium gas (right side) cases, evaluated in correspondence of trajectory peak heating (i.e., CP 2).

The streamwise station of this plane has been chosen in such a way as to clearly appreciate where the SSI on the wing takes place. The right side of Fig. 17 shows the same results in a horizontal plane passing through the wing leading edge, highlighting the bow shock trace in this plane, as well as the SSI phenomenon.

CFD results for $M_\infty = 8.5$ and AoA $= 18$ deg are shown in Fig. 18, where Mach number contours are reported in the case of equilibrium gas conditions. By comparing Figs. 17 and 18 it is possible to appreciate that the effect of the AoA for the bow shock interaction on the wing leading edge is to move the interaction region toward the tip passing from AoA $= 30$ to 18 deg. Indeed, the position of SSI changes along the atmospheric descent, depending on altitude, Mach, and AoA reentry profiles. Moreover, despite the AoA $= 18$ deg is the lowest one, no SSI on VTO fin is observed, as clearly evident looking at Mach number contours reported on the slice cutting the tail (see Fig. 18).

Regarding the consistency of predicted aerodynamic coefficients from Figs. 19–21 it can be recognized, for example, the comparison among the VTO hopper aerodynamics estimated by engineering methods and the CFD data for $M_\infty = 5$ and $M_\infty = 10$. Note that, the results recognized in Fig. 20 refer to pressure drag, because only one Navier–Stokes computation has been performed. Anyway, the CIRA experience suggests that SIM viscous results compare rather well with CFD until viscous interaction phenomena and real gas effects arise [15].

As clearly evident, results of the engineering-based approach and CFD computations compare very well at each Mach number and AoA considered, thus confirming the reliability of the booster engineering-based AEDB. The maximum difference has been found at Mach 16 and AoA $= 50$ deg, and it results within an error bar of 10% maximum.

As far as the reliability of engineering-based aeroheating is concerned, several comparisons among engineering and CFD results have been performed. As an example, through Figs. 22–25, the heat flux on the fuselage centerline and airfoil (Sec. W1) at trajectory peak heating, both for laminar and turbulent flow conditions, is provided.

Note that the CFD heat flux markedly differs from that evaluated with engineering methods, only at about $x/L_{\text{ref}} = 0.2$ and 0.8. This behavior is due to pressure changes related to surface curvature variations induced by blending of the nose (e.g., downstream effects of nose blunting that originate a combining effect of the entropy layer and AoA) and wing sections into the VTO main fuselage [13,16]. Therefore, the comparisons show the effect of local entropy values,

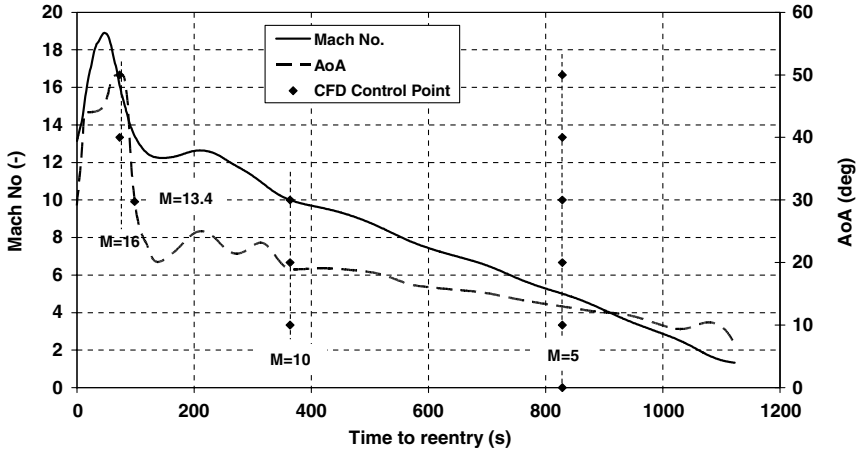

Fig. 16 The VTO hopper reentry scenario with control points for CFD analyses.

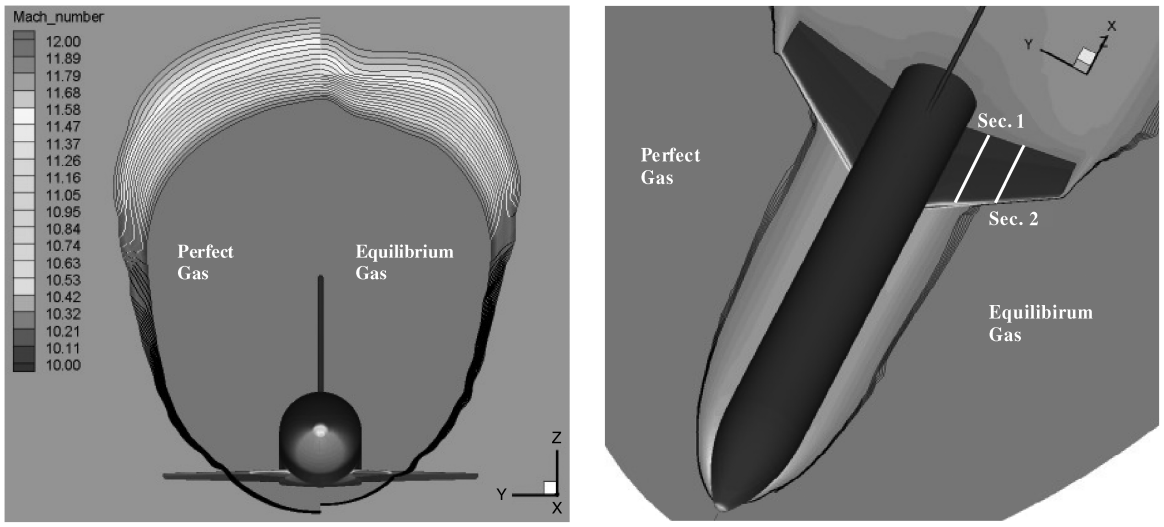

Fig. 17 Mach number contours on SSI cross planes (left). Bow shock trace on *xy* plane through WLE. Euler computation at trajectory peak heating conditions for perfect and equilibrium flow.

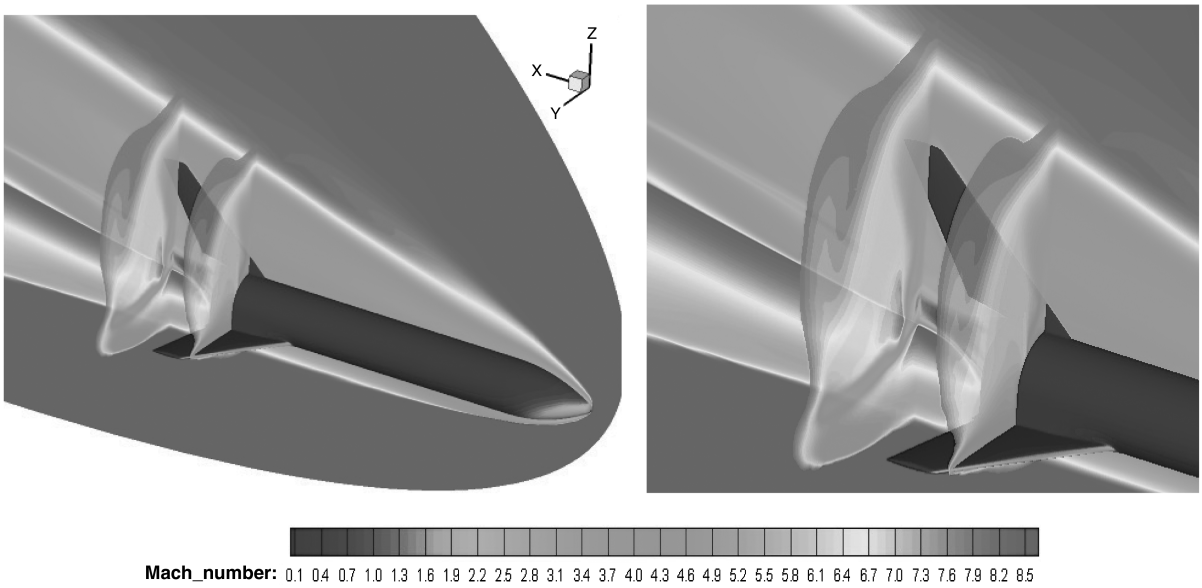

Fig. 18 Mach contours on booster's pitch plane and two cross planes. Euler computation at $M_\infty = 8.5$ and AoA = 18 deg. Equilibrium flow conditions.

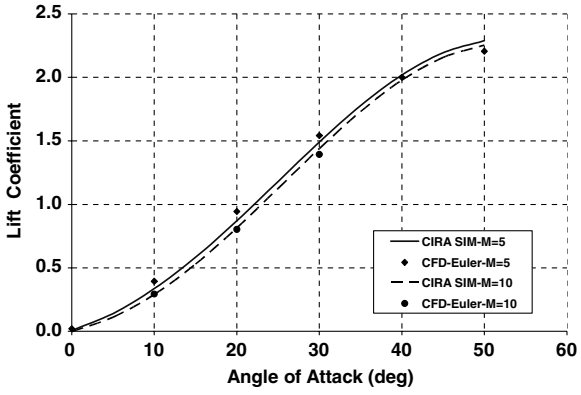

Fig. 19 Lift coefficient vs AoA. Comparison between SIM and CFD Euler at $M_\infty = 5$ and $M_\infty = 10$.

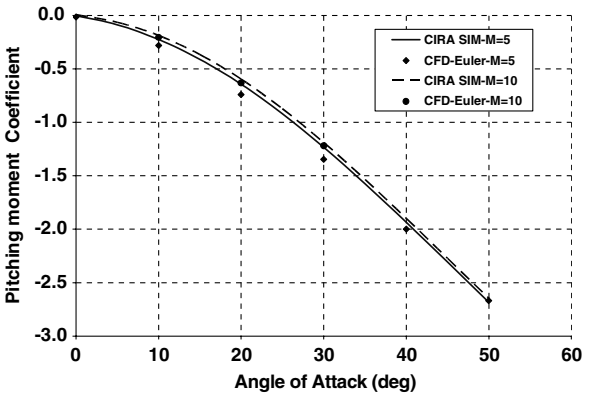

Fig. 21 Pitching moment coefficient vs AoA. Comparison between SIM and CFD Euler at $M_\infty = 5$ and $M_\infty = 10$.

thus highlighting, in addition, the fact that the CIRA approximate code considers that the shock layer is rotational only [17]. Indeed, the bow shock produced by the blunted nose facing the flow at AoA generates entropy gradients in the inviscid shock layer, thus resulting in inviscid velocity gradient normal to the VTO surface that the CIRA-SIM code does not take into account for (e.g., the entropy layer) [15,18].

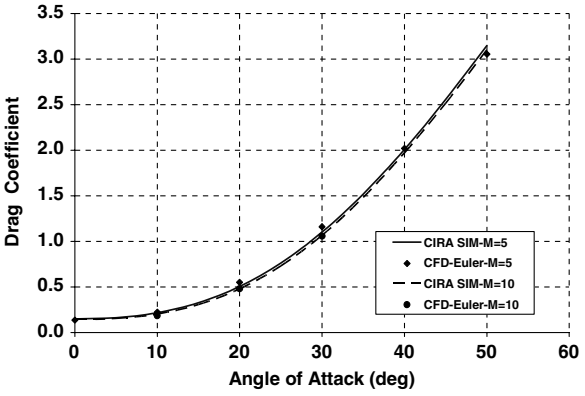

Fig. 20 Drag coefficient vs AoA. Comparison between SIM and CFD Euler at $M_\infty = 5$ and $M_\infty = 10$.

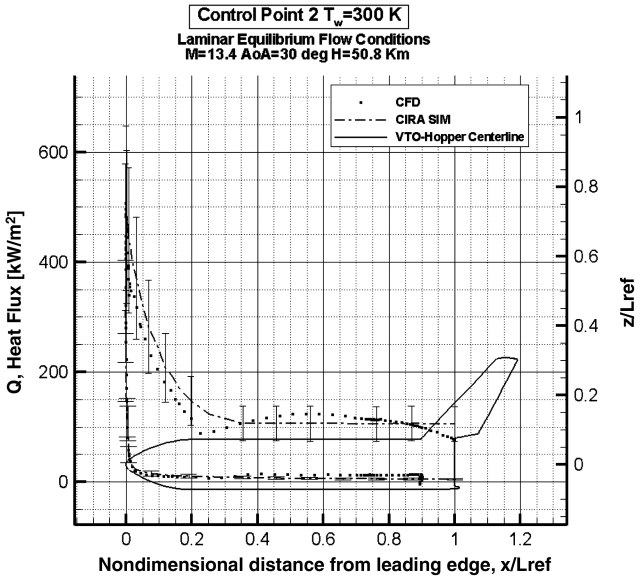

Fig. 22 Centerline heat flux (Secs. B1, B5) at peak heating (CP 2) for laminar equilibrium flow. Error bar of ±30%.

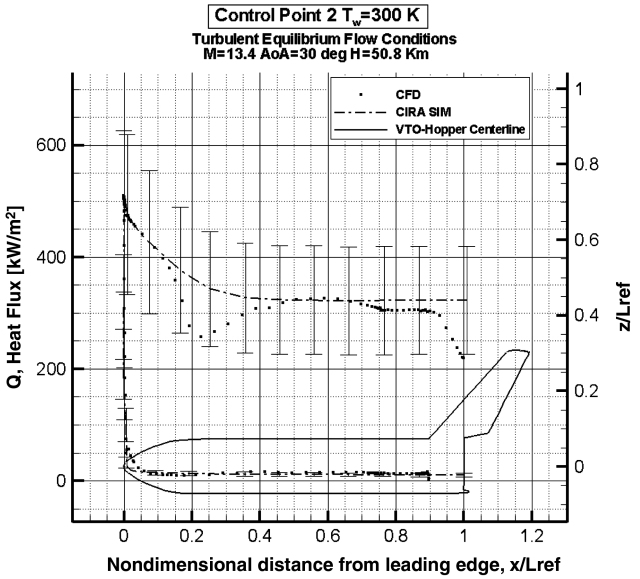

Fig. 23 Centerline heat flux (Secs. B1, B5) at peak heating (CP 2) for turbulent equilibrium flow. Error bar of ±30%.

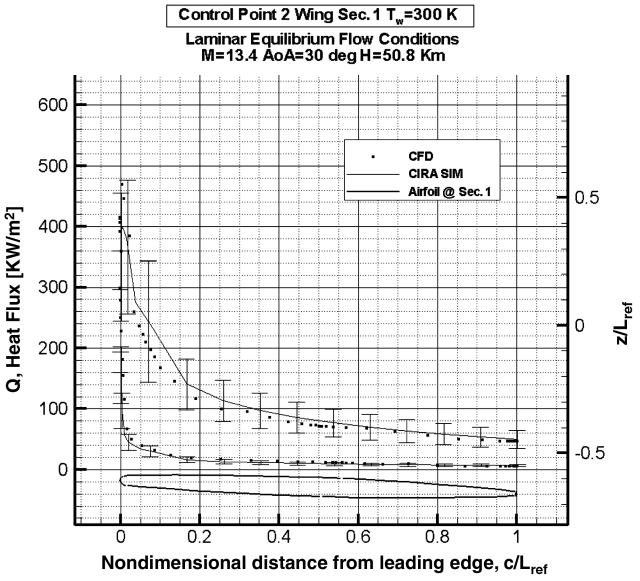

Fig. 24 Heat flux on airfoil Sec. W1 at peak heating (CP 2) for laminar equilibrium flow. Error bar of ±30%.

The aeroheating results for wing Sec. W1, reported in Figs. 24 and 25, highlight that engineering results compare rather well with CFD except for the airfoil stagnation region. Engineering analyses refer, in fact, to a wing-alone condition only, because the effects of vehicle bow shock can be considered by means of CFD analyses only.

Indeed, since the Sec. 1 airfoil is behind the vehicle bow shock (see right side of Fig. 17), it faces different flowfield conditions with respect to the freestream ones, thus experiencing heat flux higher than the one evaluated by means of 1-D BLM: the most heated zone of the wing is the one inside the bow shock.

Therefore, a reliable vehicle TPS design demands the analysis of SSI, because differences on heat flux distribution between 1-D BLM and CFD analyses are expected moving in a spanwise direction toward the tip. Moreover, the heat flux distribution on airfoil at Secs. 2 and 3 could be influenced by a vortex arising from the wing tip (that can be investigated via CFD computations only).

Anyway, it can be seen that the engineering solution, both for fuselage and wing, compares rather well with respect to the CFD one, and that, in general, it is conservative with respect to CFD results.

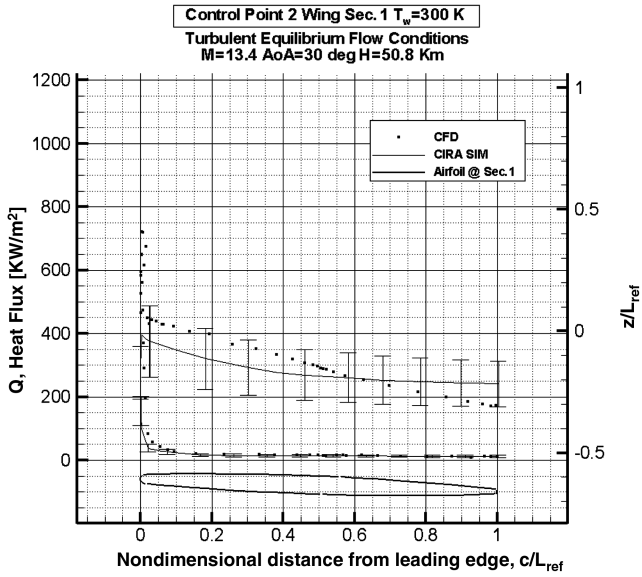

Fig. 25 Heat flux on airfoil Sec. W1 at peak heating (CP 2) for turbulent equilibrium flow. Error bar of ±30%.

However, the comparison is not so good in the regions where strong 3-D flowfield and turbulence effects exist.

In conclusion, at this early stage of vehicle design, the engineering aeroheating assessment of the VTO hopper is reliable provided that a proper margin of at least 30% is adopted with respect to the engineering data, as confirmed by error bars reported through Figs. 22–25.

VII. Conclusions

Preliminary hypersonic aerodynamics and aerothermodynamics data sets for the reusable VTO hopper concept, under investigation in the frame of the Future Launchers Preparatory Program of the European Space Agency, have been carried out in the present work. The VTO hopper aerodynamics analyses refer to Mach numbers ranging from 2 to 20 and AoA from 0 to 50 deg, which are conditions covering the whole reentry flight scenario of the vehicle concept. For the aerothermodynamic point of view, selected points of the reentry trajectory have been simulated. It is worth mentioning, however, that some results of the present analysis have not been carried out by means of accurate and more reliable CFD computations. Therefore, proper margins should be adopted in recognizing the whole vehicle aerodynamic and aerothermodynamic data.

In any case, the obtained results confirm that the difference between CFD and engineering-based design is smaller than 10% for aerodynamic coefficients, whereas a margin of about 30% has to be taken into account for what concerns the aerothermodynamic results. This fact confirms that SIM and a one-dimensional boundary-layer method represent a reasonable preliminary design approach to accomplish the aerodynamic and aerothermodynamic characterization of a reentry vehicle across the hypersonic regime.

Anyway, this work highlights interesting features for a reliable aerothermal environment definition of the FLPP concept. For example, the vehicle nose experiences a heat flux within 500 kW/m^2 while, at the wing leading edge, a higher heat flux has been predicted (up to 700 kW/m^2). Therefore, it derives that the wing TPS design is more challenging. Moreover, turbulent equilibrium flow condition results in a conservative estimation of the aerothermal environment that the vehicle has to withstand through descent, as expected.

Note, in conclusion, that further analyses seem necessary on specific topics to increase the reliability of the aerodynamic and aerothermodynamic databases, and to reduce the phase-0 design margins. In particular, the attention has to be focused on real gas and rarefaction effects, as well as on shock–shock interactions and laminar-to-turbulent transition. Real gas effects are expected to affect stability and control derivatives of vehicle, in particular, its pitching

moment. Moreover, real gas effects cause a shock that lies closer to the vehicle with respect to the position that would characterize a perfect gas case, thus influencing the SSI effect on the wing leading edge.

Further, regarding the aerodynamic coefficients, it is well known that at very high altitude, when the Reynolds number decreases and rarefaction effects are present, there is a strong increase of the drag coefficient with the consequent reduction of the maximum lift-to-drag ratio. As far as the laminar-to-turbulent transition is concerned, it is well known that it can cause strong overheating on the vehicle's surface.

References

[1] Kauffmann, J., "Future European Launch Systems in the FLPP Overview and Objectives," *57th International Astronautical Congress*, IAC-06-D2.4.05, International Astronautical Congress, Valencia, Spain, 2–6 Oct. 2006.

[2] Tomatis, C., Bouaziz, L., Franck, T., and Kauffmann, J., "RLV Candidates for European Future Launchers Preparatory Programme," *57th International Astronautical Congress*, IAC-06-D2.2.072-6, International Astronautical Congress, Valencia, Spain, Oct. 2006.

[3] Pezzella, G., Roncioni, P., Marini, M., Kauffmann, J., and Tomatis, C., "Aerodynamic and Aerothermodynamic Evaluation of the VTO Hopper Concept in the Frame of ESA Future Launchers Preparatory Programme," *15th AIAA International Space Planes and Hypersonic Systems and Technologies Conference*, AIAA, Reston, VA, 28 April–1 May 2008.

[4] Di Sotto, E., and Bastante, J. C., "Hopper Trajectories," FLPP-DME-TEC-FIR01-E-R, Deimos Engenharia, Nov. 2007.

[5] Olynick, D., "Trajectory-Based Thermal Protection System Sizing for a *n* X-33 Winged Vehicle Concept," *Journal of Spacecraft and Rockets*, Vol. 35, No. 3, May–June 1998, pp. 249–257. doi:10.2514/2.3338

[6] Prabhu, D. K., "System Design Constraints-Trajectory Aerothermal Environments," *Critical Technologies for Hypersonic Vehicle Development*, RTO AVT/VKI Lecture Series, Von Karman Institute for Fluid Dynamics, Rhode Saint Genèse, Belgium, 10–14 May 2004.

[7] Schettino, A., Pezzella, G., Gigliotti, M., De Matteis, P., Brach Prever, E., and Massobrio, F., "Aero-Thermal Trade-off Analysis of the Italian USV Re-Entry Flying Test Bed," AIAA Paper 2006-8114, Nov. 2006.

[8] Pezzella, G., Battista, F., Schettino, A., Marini, M., and De Matteis, P., "Hypersonic Aerothermal Environment Preliminary Definition of the CIRA FTB-X Reentry Vehicle," *West-East High Speed Flow Field Conference*, The ECCOMAS: European Community on Computational Methods in Applied Sciences, Mowcow, Russia, 19–22 Nov. 2007.

[9] Tauber, E. M., "A Review of High-Speed, Convective, Heat-Transfer Computation Methods," NASA TP 2914, 1989.

[10] Gomg, L., Ko, W. L., and Quinn, R. D., "Thermal Response of Space Shuttle Wing During Reentry Heating," NASA TM 85907, June 1984.

[11] Srinivasan, S., Tannehill, J. C., and Weilmuenster, K. J., "Simplified Curve Fits for the Thermodynamic Properties of Equilibrium Air," NASA Reference Publ. 1181, Aug. 1987.

[12] "Aerodynamic and Rocket-Exhaust Heating During Launch and Ascent," NASA Space Vehicle Design Criteria (Structures), NASA Langley Research Center, NASA/SP-8029, May 1969, p. 33.

[13] Weilmuenster, K. J., Gnoffo, P. A., Greene, F. A., Riley, C. J., and Hamilton, H. H., "Hypersonic Thermal Environment of a Proposed Single-Stage-to-Orbit Vehicle," *Journal of Spacecraft and Rockets*, Vol. 34, No. 6, Nov.–Dec. 1997, pp. 697–704. doi:10.2514/2.3282

[14] Bertin, J. J., *Hypersonic Aerothermodynamics*, AIAA Educational Series, AIAA, Washington, D.C., 1994.

[15] Schettino, A., Pezzella, G., Battista, F., and Votta, R., "USV_X-Phase A Aerodynamic and Aerothermodynamic Analysis," CIRA-CF-06-1393.

[16] Zoby, E. V., Moss, J. N., and Sutton, K., "Approximate Convective-Heating Equations for Hypersonic Flows," *Journal of Spacecraft and Rockets*, Vol. 18, No. 1, Jan.–Feb. 1981, pp. 64–70. doi:10.2514/3.57788

[17] Zoby, E. V., and Thompson, A., "Flowfield and Vehicle Parameter Influence on Hypersonic Heat Transfer and Drag," *Journal of Spacecraft and Rockets*, Vol. 27, No. 4, July–Aug. 1990, pp. 361–368. doi:10.2514/3.26151

[18] Wurster, K. E., Zoby, E. V., and Thompson, R. A., "Flowfield and Vehicle Parameter Influence on Results of Engineering Aerothermal Methods," *Journal of Spacecraft and Rockets*, Vol. 28, No. 1, Jan.–Feb. 1991, pp. 16–22. doi:10.2514/3.26203

G. Palmer
Associate Editor